Thickness and roughness of transparent gold-palladium anodes have no impact on growth kinetics and yield coefficients of early-stage *G. sulfurreducens* biofilms

Francesco Scarabotti[1], Katja Bühler[2], Matthias Schmidt[3] and Falk Harnisch[1]*

[1]Department of Environmental Microbiology, Helmholtz-Centre for Environmental Research - UFZ, Leipzig, Germany
[2]Department Solar Materials, Helmholtz-Centre for Environmental Research - UFZ, Leipzig, Germany
[3] Department of Isotope Biogeochemistry, Helmholtz-Centre for Environmental Research – UFZ, Leipzig, Germany

*corresponding author: F. Harnisch, falk.harnisch@ufz.de

Abstract:

Geobacter sulfurreducens is the model organism for electroactive microorganisms performing direct extracellular electron transfer and forming thick mature biofilm electrodes. Although numerous physiological properties of mature biofilm electrodes are deciphered, there is an extensive gap of knowledge on the early-stage biofilm formation. We have shown recently that transparent gold-palladium (AuPd) electrodes allow for analysis of early-stage biofilm formation using confocal laser scanning microscopy. Here we analysed the influence of thickness (ranging from 12.5 to 200 nm) and roughness of AuPd electrodes on physiological parameters of *G. sulfurreducens* early-stage biofilms. We show that when grown potentiostatically at -200 mV vs. Ag/ AgCl sat. KCl neither maximum current density (j_{max} of ~ 80-150 µA cm^{-2}) nor *lag* time (*lag t* of ~ 0.2-0.4 days) or single cell yield coefficients (Y_{Ne} of 1.43 × 10^{12} cells mol_{e-}^{-1}) of the biofilms are influenced by the electrode preparation. This confirms the robustness of the experimental approach, which is an inevitable prerequisite for obtaining reliable results in follow-up experiments.

Key words:

Microbial electrochemical technology, *Geobacter*, electroactive microorganism, yield coefficient, confocal laser scanning microscopy

Introduction:

Electroactive microorganisms (EAM) utilize solid-state materials as terminal electron acceptors (TEA), which is known as extracellular electron transfer (EET). TEA include, for instance, minerals formed of Fe (III), Mn (III) or Mn (IV) [1] as well as anodes made of metal or carbon. When anodes are serving as TEA, they provide an immediate link between the intracellular metabolic electron flow and the external flow of electric current. The two main modes of EET are direct EET and indirect (or mediated) EET. Both modes allow for EET between microorganisms and solid-state materials as well as in between microorganisms. The latter includes, for instance, direct interspecies electron transfer (DIET) that was shown for the first time in co-cultures of *Geobacter metallireducens* and *Geobacter sulfurreducens*. Here, ethanol served as electron donor and was utilized by *Geobacter metallireducens,* while fumarate served as final electron acceptor and was utilized by *Geobacter sulfurreducens*. Both microorganisms were metabolically coupled via DIET [2–4]. *Geobacteraceae* are one, if not the family of model organisms for EAM utilizing direct EET, including *Geobacter sulfurreducens*, that is certainly the most extensively studied EAM [5]. For direct EET, a physical contact between the outer membrane cytochromes, and hence *G. sulfurreducens* cells, and the electrode is required which leads to the formation of biofilms thereon. The anode biofilms formed by *G. sulfurreducens* are up to 100 µm thick and of high electrical conductivity [6,7]. Many details of EET of *G. sulfurreducens* are deciphered, for instance the proteins and cytochromes being mainly involved [8–11]. Yet, surprisingly, basic physiological information about the “sessile” living style of *G. sulfurreducens* as anodic biofilm is still unknown.

For a systematic physiological assessment of EAM parameters such as kinetics of growth and yield coefficients (Y_{Ne}) have to be determined. With this information available, growing electroactive biofilms at electrodes will allow for a systematic characterization and comparison of different EAM. Further, it will allow both, i) the comparison between different EAM when using an electrode or other TEA, and ii) benchmarking the metabolic performance of EAM while growing at electrodes at the identical conditions. Noteworthy, several studies already focused on the determination of these parameters for EAM, but their majority did so using TEA other than electrodes [12]. For example, Brown *et al.* reported yield coefficients of *G. sulfurreducens* growing on acetate or hydrogen as electron donor and Fe(III) as TEA [13]. It is clear that growth in planktonic culture is a very different living style and environment than as biofilm electrode. The scarcity of the physiological information for biofilm electrodes can be assigned to the fact that these are usually not accessible with available techniques. For instance the required primary information is foremost the cell number or biomass that is routinely measured as optical density for instance at 600 nm (OD_{600}). Yet, measuring OD_{600} of the solution hosting a *G. sulfurreducens* biofilm anode will provide no useful information, as almost all cells are embedded in the biofilm. Thus, methods are required to determine either biomass, intended as the combination of cells and matrix of exopolymeric substances (EPS) or cell number per area of electrode. Biomass determination, in terms of biomass dry weight, is one of the most common parameters [14–16]. Microscopy can serve as a means to measure biomass and to quantify cells on electrodes. Here, invasive and non-invasive microscopy needs to be distinguished. In the first case extensive sample preparation is required, preventing *in vivo* or even online analysis, like for scanning electron microscopy. Other, non-invasive, methods include optical microscopy, fluorescence microscopy, confocal laser scanning microscopy (CLSM) or confocal Raman microscopy (CRM) [17], and allow for *in vivo* analysis of the respective specimen [18]. However, apart from CRM, that is based on chemical markers being intrinsic to only some microorganisms, these often require electrode materials being sufficiently transparent as well as electrically conductive. These requirements limit the choice of materials significantly and thus indium tin oxide (ITO) [19] and fluorine doped tin oxide or transparent gold-based materials are the most widespread transparent electrode materials. In our previous study, we have shown that the cell number of early-stage biofilms of *G. sulfurreducens* growing on transparent gold palladium (AuPd) anodes can be well estimated via the biovolume, which can be assumed as a more precise measure in comparison to biofilm thickness, considering especially non uniform biofilms [20]. This allows to determine single cell yield coefficients (Y_{Ne}), expressed in number of cells per moles of electrons (cells $mol_{e^-}^{-1}$) transferred to the electrode and to evaluate how this parameter is influenced by the applied anode potential. Thus, the question arises, to which extent the electrode properties influence the microbial physiology. Therefore, in this study the influence of different thicknesses of the AuPd layers as well as the chemical polishing of the electrodes with Fenton reagent [21,22] on the physiology of early-stage biofilms of *G. sulfurreducens* was evaluated.

Materials and methods:

All chemicals were of at least analytical grade and were supplied from Carl Roth GmbH (Karlsruhe, Germany) and Merck KGaA (Darmstadt, Germany). De-ionized water (Millipore, Darmstadt, Germany) was used to prepare the sterile microbial media, substrate and buffer solutions. All potentials provided in this article refer to the Ag/AgCl sat. KCl reference electrode (+197 mV vs. standard hydrogen electrode, SHE).

2.1. Microorganism and cultivation media

Geobacter sulfurreducens was precultured in minimal medium containing 0.13 g L^{-1} KCl, 0.31 g L^{-1} NH_4Cl, 2.69 g L^{-1} $NaH_2PO_4 \times H_2O$, 4.33 g L^{-1} Na_2HPO_4, 12.5 mL L^{-1} of trace metal, 12.5 mL L^{-1} of vitamin solutions [23–26]; 20 mM acetate and 40 mM fumarate were added as the electron donor and electron acceptor respectively. For the electrochemical experiments 5 mM of acetate was added to the minimal medium as the only electron donor and no fumarate was supplied. To ensure anaerobic conditions the medium was purged with nitrogen gas for 30 min prior to use.

2.2. Electrochemical experiments: Setup, equipment and biofilm cultivation

All electrochemical experiments described in this study were performed in a double chamber 250 mL four-neck round-bottom flasks (Lenz Laborglas GmbH & CO.KG, Germany) using transparent AuPd working electrodes (WE) with a surface area of 3.75 cm^2 as anodes, as previously described [20] (see **Scheme 1**), a graphite rod as counter electrode (5 mm diameter, exposed surface of 4.12 cm^2, CP Handels GmbH, Wachtberg, Germany) and an Ag/AgCl sat. KCl as reference electrode (+197 mV vs. SHE, SE 11 Xylem Analytics Germany Sales GmbH & Co/Meinsberg Sensortechnik GmbH, Germany). The WE were prepared with different AuPd layer thickness and surface chemical treatment (see section 2.4). The electrical connections were made from stainless steel wires (0.6 mm diameter, Goodfellow GmbH, Friedberg, Germany), being tin soldered on the WE and inserted into counter electrode. All the connections and wires were insulated with epoxy resin (HT2, R&G Faserverbundwerkstoffe, Germany) and shrinking tube (Shrink-kon®, ABB, Germany) and the resistance of each electrode was measured using a digital multimeter (Voltcraft, VC270, Germany). The graphite counter electrodes were treated prior to use with sand paper (P220, Vitex, VSM), then rinsed with 80 % Et-OH and de-ionized water. All electrodes were tightly inserted through chloroprene stoppers (Deutsch & Neumann GmbH, Germany). The counter electrode was located in a 15 mL cathodic chamber, containing sterile minimal medium without the addition of acetate. The cathodic chamber was physically separated, but ionically connected to the anodic chamber via a cation exchange membrane (fumasep®FKE, Fumatech, Bietigheim-Bissingen, Germany). The assembled reactors were sterilized by autoclaving, except for the electrodes. Counter and reference electrodes were sterilized in Beckmann solution (625 mL of 99% Et-OH and 6.25 mL of concentrated H_2SO_4 filled to 1 L with deionized water) for 30 min and the WE were sterilized with UV light (30 min per side). The reactors were filled with 240 mL sterile mineral medium containing 5 mM acetate as electron donor and inoculated with 10 mL of a 72 h old *G. sulfurreducens* preculture (OD_{600}~ 0.6-0.7). The reactors were operated potentiostatically (MPG-2, Bio-Logic Science Instruments, Claix, France) using chronoamperometry at -200 mV. Temperature and stirring were controlled at 30°C and 150 rpm, respectively. Biofilm cultivation was performed in accordance to our previous study [20] for at least 12 days, in addition cultivation for 16 h was performed to assess very early-stage biofilm formation.

The maximum current densities (j_{max}) normalized per anodic geometric surfaces (being µA cm^{-2}) were calculated after 12 days of cultivation. The *lag* time (*lag t*), being the time expressed in days needed by the biofilms for delivering a current density of 1 µA cm^{-2}, was gained from the combined data sets for cultivating biofilms for 16 h and at least 12 days.

2.3 Preparation and electrochemical, electric and optical characterisation of AuPd electrodes

The transparent AuPd WE were prepared as previously described [20]. In brief, microscopy glass coverslips 20 mm x 20 mm (art.no. 7695024, TH Geyer, Germany) were sputter-coated with 10 nm of Chromium (sputter target from AEM deposition) as adhesion layer and subsequently with a layer of AuPd (Leica Target GoldPalladium 80/20%, DN 54 × 0.17 mm, 99.99%, 17.9 g cm^{-1}, Art. nr. 167715691, Leica Mikrosysteme Vertrieb GmbH, Wetzlar, Germany) of different thickness, namely 12.5, 25, 50, 100 and 200 nm (see **Scheme 1B**) using a sputter-coater (Leica EM SCD 500). The thickness was measured during the sputter-process with a calibrated quartz monitor (EM QSG100 Quartz Crystal Film Thickness Monitor). The electrical resistance of each electrode was measured before each experiment (see **Table 1**). Further, cyclic voltammetry (CV) in 10 mM $K_4Fe(CN)_6 \times 3H_2O$ (in minimal medium) was performed on each electrode before (abiotic, blank) and after each experiment (in the presence of biofilm) from -500 mV to +800 mV with a scan rate of 50 mV s^{-1} (see supplementary information, **Figure S1**)
To assess the light transmission UV-VIS spectrum was recorded between 220 nm and 800 nm (photoLab® 6600 UV-VIS series) (see supplementary information, **Figure S2**).

Table 1: Measured resistance, surface grain diameter (see supplementary information), *lag t* and j_{max} of the AuPd electrodes with n providing the number of independent replicates.

Electrode	R** / Ω	Grain diameter* / nm	*lag t* **/d	j_{max}***/ µA cm^{-2}	E_f**/ mV
AuPd 12.5 nm	95.07 ± 23.55 (n=7)	10.89 ± 0.06 (n=3)	0.38 ± 0.27 (n=7)	135.21 ± 36.45 (n=4)	-329.58 ± 26.28 (n=6)
AuPd 25 nm	35.69 ± 3.88 (n=7)	12.92 ± 0.17 (n=4)	0.24 ± 0.26 (n=7)	83.68 ± 19.12 (n=4)	-327.11 ± 23.54 (n=7)

AuPd 50 nm	17.37 ± 4.47 (n=7)	12.91 ± 0.22 (n=4)	0.30 ± 0.21 (n=7)	163.14 ± 25.59 (n=4)	-327.66 ± 20.07 (n=7)
AuPd 100 nm	8.35 ± 2.07 (n=6)	13.39 ± 0.28 (n=4)	0.30 ± 0.24 (n=6)	154.22 ± 20.90 (n=3)	-311.90 ± 59.28 (n=5)
AuPd 100 nm + Fenton	7.37 ± 1.01 (n=3)	12.31 ± 0.78 (n=11)	0.38 ± 0.33 (n=3)	162.67 ± 40.37 (n=3)	-316.35 ± 16.06 (n=3)
AuPd 200 nm	4.57 ± 0.90 (n=6)	15.18 ± 0.38 (n=3)	0.42 ± 0.24 (n=6)	159.60 ± 28.64 (n=3)	-300.59 ± 33.69 (n=6)

*: average and standard error from the analysis of at least three FE-SEM pictures made on the same electrode in three different fields-of-view.

** Combined data from biofilm experiments lasting 16 h as well as at least 12 days.

*** Data from biofilm experiments lasting at least 12 days.

2.4 Chemical polishing of AuPd electrodes with Fenton reagent

Chemical polishing with Fenton reagent of AuPd WE with 100 nm AuPd thickness layer was performed according to Nowicka et al. [22,21]. Therefore, the Fenton reagent was prepared always freshly and the AuPd electrodes were treated for 30 min; afterwards, they were rinsed with deionized water and utilized for biofilm cultivation (see section 2.2).

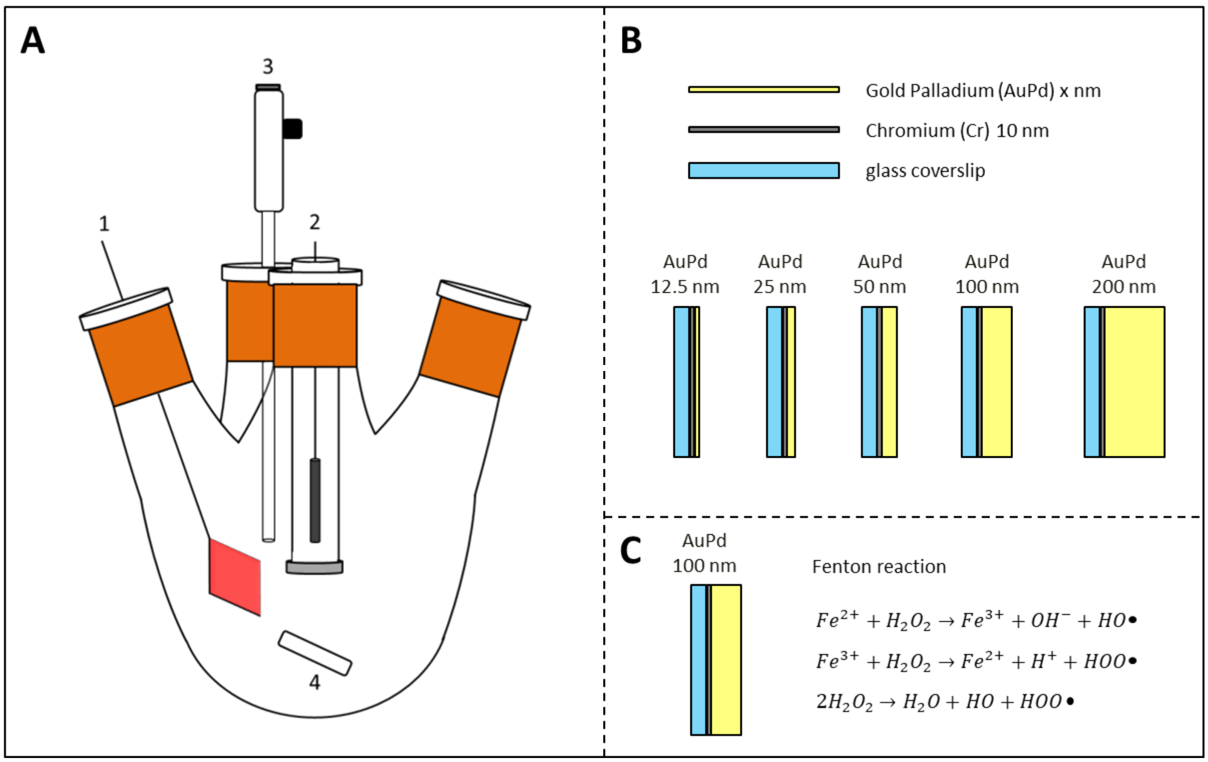

Scheme 1: (A) electrochemical double chamber batch reactor with a transparent AuPd electrode as working electrode (WE) (1), a graphite rod as CE (2) and an Ag/AgCl sat. KCl as RE (3); (B) transparent AuPd WE with different thickness of the AuPd layers (12.5 nm, 25 nm, 50 nm, 100 nm and 200 nm); (C) surface treatment of AuPd electrodes with Fenton reagent.

2.5 Chemical analysis

The acetate concentration was analyzed before and after each batch cultivation experiment for the determination of coulombic efficiencies (see supplementary information, **Figure S3**). For that, a high-performance liquid chromatograph (HPLC, Shimadzu Scientific Instruments, Kyoto, Japan) equipped with a photodiode array detector (SPD-M20A prominence, Shimadzu Scientific Instruments, Kyoto, Japan), a

Hi-Plex H column (300 mm x 7.7 mm ID, 8 µm pore size, Agilent Technologies, Santa Clara, USA) and a pre-column (Carbo-H 4 mm x 3 mm ID, Security Guard, Torrance, Phenomenex) were used. Isocratic elution at 65 °C with 5 mmol L^{-1} H_2SO_4 (0.01 N) as eluent was set at flow rate of 0.6 mL min^{-1} for 30 min. Peak identification and calibration of acetate was carried out with external standards (5.33 mg L^{-1} to 861.24 mg L^{-1}, six point calibration; R^2 = 0.99). All measured concentrations were within the range of the calibration curve. Prior to analysis samples were centrifuged at 15700 rcf for 3 min and filtered with a 0.2 µm PTFE filter (VWR international, Germany).

2.6 Field-Emission Scanning Electron Microscopy analysis

Microscopic imaging of as-prepared electrodes as well as biofilm over-grown ones was performed with a Zeiss Merlin VP Compact (Carl Zeiss Microscopy, Oberkochen, Germany) field-emission scanning electron microscope (FE-SEM) equipped with the software SmartSEM for image acquisition. The nano-texture of the as-prepared electrodes was investigated without any further preparation at a magnification of 80,000X and an electron acceleration voltage of 10 kV. The beam-current amounted to approx. 250pA. The biofilms on the electrodes were investigated at a magnification of 2,000X. Because of the low electron-density of the bio-matter a lower electron acceleration voltage of 2kV was chosen here in order to be more surface-sensitive and avoid cells to appear semi-transparent in the micrographs.

In order to maintain the structural integrity of the microbial cells the biotic electrodes, i.e. early-stage biofilm electrodes after 16 h of electrode polarization, were fixed in 5 mL of 2 % glutaraldehyde solution for 1 h in the dark, then rinsed with deionized water and dehydrated in growing concentrations of ethanol (30 %, 50 %, 70%, 80%, 90% and 100 %; 5 min per each concentration) and subsequently air-dried prior to electron microscopy imaging.

2.6.1 FE-SEM image analysis of abiotic electrodes

The grain-sizes of the surfaces of the as-prepared electrodes with differently thick AuPd-coating were analyzed by imaging at least three fields-of-view by FE-SEM. The “naked” surface of the electrodes showed a grainy texture (see supplementary information, **Figure S4** and **Figure S5**).The micrographs were then analyzed with the well-known image-processing software ImageJ (ImageJ 1.45s, Java 1.8.0_202, 32-bit). Briefly, the micrographs were imported as image sequence and calibrated to physical length units. Subsequently the image sequence was duplicated and a Gaussian Blur filter with a Sigma (Radius) of 20 was applied to the duplicates. After conversion to 32-bit precision the original images were then divided by the blurred ones in order to remove the background. Segmentation was carried out by thresholding, with the option “dark background” selected and applying “watershed”. This separated the grains such that the function “analyze particles” (10 nm^2-infinity) could be used for counting and binning them. The calculated grain diameter per electrode is shown in **Table 1**.

Per each field-of-view one average grain surface value is obtained. The grain diameter is then calculated assuming a circular grain area and the values reported are the averages and standard error coming from at least three fields-of-view.

2.6.2 FE-SEM image analysis of early-stage polarization electrodes (16h)

For each of the biofilm-overgrown electrodes three biological replicates were investigated by FE-SEM in order to determine the areal cell-density. Per electrode at least nine micrographs were acquired and analyzed. As before image analysis was performed with the software ImageJ. Again the images were imported as image sequence and the background was subtracted. For that the function "Subtract Background" was employed using a rolling ball radius of 1000 px and the option "Light background". Segmentation was carried out by B&W thresholding with the options "Calculate Threshold for Each Image" and "Black Background" selected, and using the function "Watershed" to segment the attached cells. Finally, cells were counted with the function "Analyze Particles" using particle sizes from 100 px^2 to infinity. Cells on the edges were excluded from counting and the "Outlines" function was used for checking the accuracy of the cell counting. From each set of at least nine micrographs averaged real cell densities (cells per cm^2) are calculated and used for the calculation of the reported areal cell densities (d_{cell}) and their standard deviations that are shown in **Figure 1**. Representative micrographs are shown in **Figure S6**. The chronoamperometry of the early-stage polarization electrodes (16h) is available in the supplementary information (see **Figure S7**).

2.7 Confocal laser microscopy and calculation of single cell yield coefficients

The WE were analyzed with CLSM as previously described [20]. Briefly, after each electrochemical cultivation the WE were carefully transferred in petri dish with the biofilm facing to the top and covered by a staining solution containing 475 µL of minimal medium and 25 µL of SYTO-9 (ThermoFischer®, Germany). After 15 min of incubation in the dark the biofilm anodes were washed three times with fresh minimal medium (500 µL per each washing step) and mounted on a dip slide (TH Geyer, Germany). A Zeiss LSM 710 NLO confocal laser microscope (Jena, Germany) equipped with a 488 nm laser line for the excitation of SYTO-9 was used for image acquisition. Stacks of images were taken with a Plan Apochromat 10X/0.45 W objective and an Axiocam 503 color. 3D image reconstruction and analysis were performed with IMARIS (version 8.2.0, dec 15, 2015, build 38,338 for x64, Bitplane AG, Zurich, Switzerland). Single cell yield coefficients expressed in cells per mol_{e-}^{-1} (Y_{Ne}, Eq. 1), are calculated as previously described assuming that the presence of eDNA in the EPS is negligible and thus not affecting the fluorescence signal significantly [9,10].

$$Y_{Ne} = slope \times F \qquad (1)$$

with slope as the angular coefficient of the linear regression on data points plotted as produced charge density (q, being C cm^{-2}) on x axis and the cell density (d_{cell}, being cells cm^{-2}) on y axis and F as the Faraday constant (96,485 C mol_{e-}^{-1}).

2.8 Statistical analysis

All reported experiments were performed at least in biological triplicate. Average values and standard deviations are reported with *n* in brackets as the number of independent replicates. Analysis of variance (ANOVA-one way) was applied for checking, if the slightly differences observed in **Figure 1**, regarding the cell density calculation on the AuPd electrodes were significant (α=0.01); and Tuchey test (α=0.01) was applied for comparing the means of the observed j_{max} and for checking if they significantly differed.

<u>3. Results and discussion:</u>

3.1 The influence of different AuPd thickness on *lag* time and maximum current density

Figure 2A shows the results of the chronoamperometric cultivation of *G. sulfurreducens* at - 200mV in double chamber electrochemical reactors. No significant difference in terms of maximum current densities (j_{max}) and *lag* phases (*lag t*) was observed amongst electrodes with different AuPd layer thicknesses. One may argue that the different ohmic resistance of the electrodes (see **Table 1**) may impact the electrochemical performance. However, it is of note that all experiments were conducted under potentiostatic control and the maximum potential gradient across the entire electrode is calculated to be 71 mV (for 12.5 nm thick electrodes at 200 µA cm^{-2}). As **Table 1** summarizes, the observed *lag t* were constant at a ~ 0.2-0.4 days. Also no significant difference could be observed for the j_{max}, which were of about 150 µA cm^{-2}. A slight difference, being not significant when using Tuchey test (α=0.01), was only found for the AuPd 25 nm electrodes, which exhibited a j_{max} of 83.68 ± 19.12 µA cm^{-2}. These values are higher than the 17.23 ± 23.30 µA cm^{-2} that we reported in our previous study for *G. sulfurreducens* grown at the applied anode potential of -200 mV in double chamber reactors at AuPd 25 nm electrodes [20]. Also the *lag t* significantly decreased from 6-7 days to 0.2-0.4 days. These differences could be explained by the 2.5 times higher volume to surface area ratio in this study. In addition to the surface thickness, the effect of chemical polishing of AuPd electrodes with Fenton reagent was analyzed. According to Nowicka *et al.* [22,21] the treatment of gold surfaces with Fenton reagent yields a fully polished, absolute smooth surface. The chemical polishing was exemplary studied at 100 nm AuPd electrodes, as unpolished these possess a comparable high grain surface diameter of 13.39 ± 0.28 nm (see **Table 1**) and still a sufficient transparency that would allow also optical microscopy (see **Figure S2**). The polished 100 nm AuPd electrodes exhibited an only slightly grain surface diameter of 12.31 ± 0.78 nm (see **Table 1**). Thus, as can be expected and as **Figure 2B** shows also in case of the chemically polished electrodes no significant difference could be observed. As summarized in **Table 1** the j_{max} and *lag t* were 162.67 ± 40.37 µA cm^{-2} and 0.38 ± 0.33 days respectively, which are not significantly different from the values obtained for untreated 100 nm AuPd (j_{max} of 154.22 ± 20.90 µA cm^{-2}; *lag t* of 0.30 ± 0.24 days). This confirms that further polishing in the sub-micron level does neither influence the biofilm performance nor EET thermodynamics. However, we speculate that the effect of chemical polishing might be more pronounced for rougher or even 3D-structured gold electrodes, e.g. using micro-pillar structures [27]

The results differ to some extent with literature. For instance, Liu *et al.* [28] showed that for an anode potential of +242 mV vs. SHE (that is +43 mV vs Ag/AgCl sat. KCl) *G. sulfurreducens* started the current production after 10-30 hours (~0.42-1.25 days) and yielded a j_{max} of ~1600 µA cm^{-2} for Au array electrodes and of ~400 µA cm^{-2} for rectangular Au electrodes within the first 140 hours of growth (5.83 days). Here, the obtained results are more comparable to the rectangular Au electrodes; however, we observed values of j_{max} being approximately 3 times lower. This difference can be explained by the more positive applied anode potential of Liu et al. [28], the 6 times higher concentration of acetate of 30 mM, but especially the utilization of a single chamber system. In comparison to the here used double chamber system, in single chamber systems hydrogen produced at the counter electrode is available for the biofilm at the anode and hence can be further utilized as source of electrons by *G. sulfurreducens* [5,29,20].

In addition to that no influence could be observed in the formal potential (E_f) of the EET, which remained constant at -300 to -330 mV (see **Table 1**) as already shown [30,31]. The observed coulombic efficiencies were well in line with literature (see supplementary information, **Figure S3**).

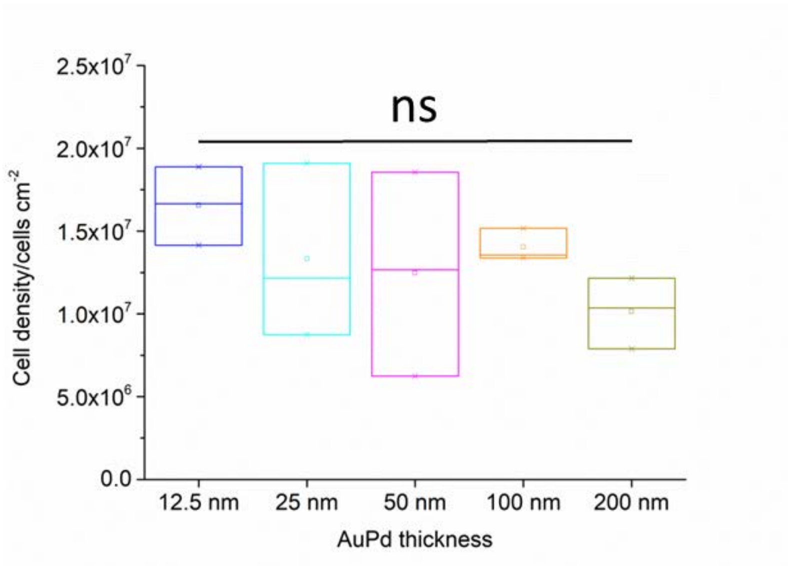

Figure 1: Box plot showing the cell density determination of very early-stage biofilms (16 h) of *G. sulfurreducens* on 12.5 nm (blue), 25 nm (cyan), 50 nm (magenta), 100 nm (orange) and 200 nm (dark green) AuPd electrodes. No significant difference could be observed between the different experimental conditions (ns).

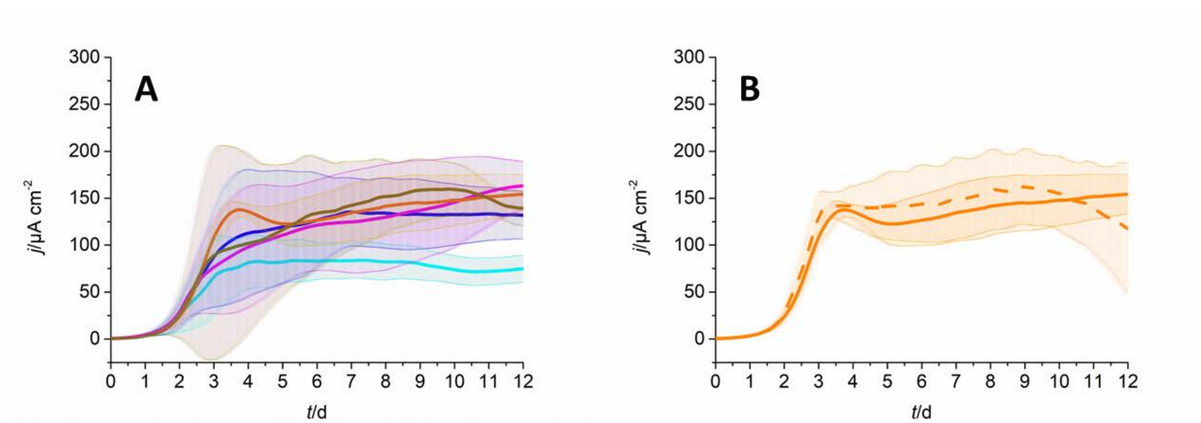

Figure 2: Chronoamperometric cultivation at -200mV of *G. sulfurreducens* in double chamber electrochemical reactors using different working electrodes (WE): (A) AuPd with thickness of 12.5 nm

(blue line, n=4), 25 nm (cyan line, n=4), 50 nm (magenta line, n=4), 100 nm (orange line, n=3) and 200 nm (dark green line, n=3); and (B) AuPd with thickness of 100 nm being chemically polished using Fenton reagent (dashed orange line, n=3) (see section 2.4), for comparison untreated electrodes (continuous orange line) are shown. Shadowed areas indicate standard deviations.

3.4 Single cell yield coefficients

Neither the kinetics of biofilm growth, as shown above, nor the electrochemical reversibility of the redox probe ferri/ferro-cyanide was influenced by the electrode preparation (see cyclic voltammetry in supplementary information, **Figure S1**). Thus, the question that needed to be answered was, if the metabolic efficiency is influenced by the electrode material. As expected, by increasing the thickness of the AuPd layer the light transmission of the electrodes decreased. Optical microscopy is possible for thicknesses of up to 100 nm. Yet, for all materials it was possible to apply confocal laser scanning microscopy (CLSM), if the excitation laser is hitting directly the biofilm and the microscope objective is located to the biofilm side (see section 2.8).

Single cell yield coefficients were calculated using CLSM (see section 2.7). **Figure 3A** shows the charge density to cell density plot for all tested electrode materials as well as one data point from our previous study for the same conditions [20]. As no significant difference was observed, the data from this study was pooled for further calculations as **Figure 3B** shows. The pooled data led to single cell yield coefficients of 1.43×10^{12} cells $mol_{e^-}^{-1}$, which is in good agreement with previous studies (see **Table 2)**. Note, that possible effects by EPS are neglected here.

To increase comparability with literature and to shed light on very early-stage biofilm formation we quantified the cell density of *G. sulfurreducens* on electrodes polarized for only 16 h. This was possible by means of field-emission scanning electron microscopy, as shown in Füeg et al. [32]. The results of this analysis can be observed in **Figure 1**. As expected no significant difference of cell density was observed for the tested electrode materials with $1.0\text{-}1.5 \times 10^{7}$ cells cm^{-2} of electrode area at a charge density of 0.03-0.13 C cm^{-2} (see also red inset in **Figure 3A**).

The cell densities calculated from this analysis were included in **Figure 3A, B** for single cell yield coefficients determination and shown separately in **Figure S8**, representing the red marked area in **Figure 3A.**

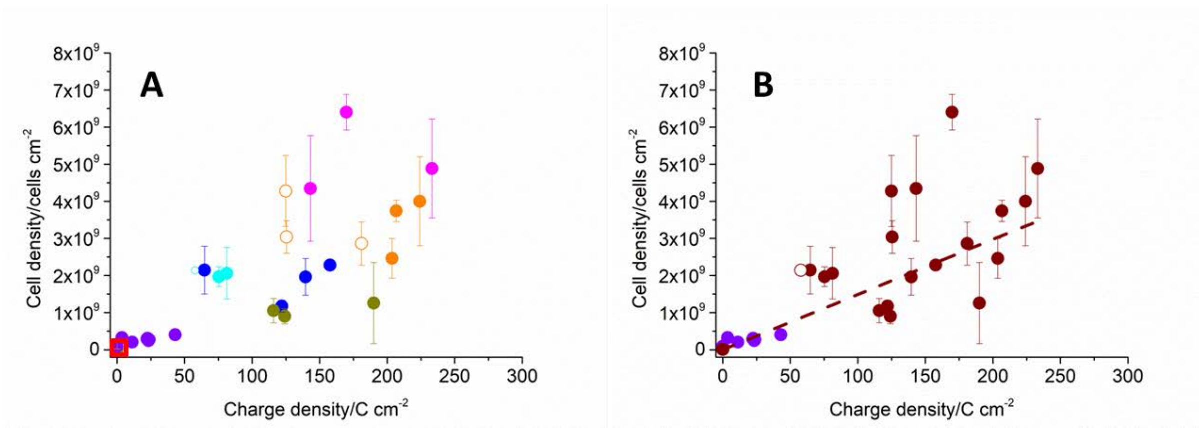

Figure 3: (A): charge density to cell density plot of *G.sulfurreducens* grown in double chamber reactors at the applied anode potential of -200 mV (vs Ag/AgCl sat. KCl) indicating data coming from [20] in violet, AuPd 12.5 nm electrodes (blue points), AuPd 25 nm electrodes (cyan points), AuPd 50 nm (magenta points), AuPd 100 nm (filled and empty orange points respectively) and AuPd 200 nm electrodes (dark green points). A zoomed view of the red region in A, which show the data points calculated from the early-stage polarized biofilms (16 h), is available in **Figure S8.** (B): data points from (A) from the different AuPd thickness electrodes pooled together (brown points) and from [20] (violet points). Linear regression is applied for the determination of single cell yield coefficients, according to section 2.8. Error bars indicated the standard error coming from the biofilm volume determination in three different areas of the same electrode. The empty cyan data point in (A), which correspond to the empty brown data point in (B) is excluded from the linear regression as for technical reasons just one picture could be acquired.

Table 2: Yield coefficients of *G. sulfurreducens* grown on transparent AuPd electrodes in double chamber reactors calculated according to section 2.8.

E/mV	Y_{Ne}/cells $mol_{e^-}^{-1}$	Standard Error (SE), Y_{Ne}/cells $mol_{e^-}^{-1}$	r	Adj. R^2	Reference
-200	1.43×10^{12}	1.52×10^{11}	0.86	0.73	this study
-200	1.15×10^{12}	8.83×10^{10}	0.98	0.95	[20]

Conclusions:

In this study we showed that different thicknesses ranging from 12.5 nm to 200 nm of AuPd electrodes as well as their chemical polishing using Fenton reagent:

i) Does not influence the electrochemical performance parameters (j_{max} and the *lag t)* as well as the formal potential of the extracellular electron transfer (E_f) of early-stage biofilms of *G. sulfurreducens;*

ii) Does not impact the physiology of formation of early-stage of *G. sulfurreducens* biofilm anodes in terms of cell density d_{cell} and Y_{Ne} , which remains comparable to the yield coefficients we calculated in our previous study [20].

Optical microscopy can be applied to AuPd electrodes with thicknesses of up to 100 nm (see supplementary information, **Figure S2**), while CLSM or any kind of fluorescence microscopy can be applied also for thicker layers of AuPd, if the objective and the excitation laser are facing the biological specimen (cells, biofilms).

Thus, we conclude that AuPd electrodes are very useful and promising material allowing a robust and unbiased growth and analysis of *G. sulfurreducens* biofilms. Thus, these need to be further exploited, for instance for the determination of single cell yield coefficients of other biofilm-forming EAM. Therefore, the here developed platform may serve as an excellent foundation, but specific features of the metabolism and EET of these EAM must be taken into account. We further foresee their use to explore the ecology of EAM, for instance studying the priority effect [33,34].

Acknowledgements

The authors acknowledge Mahir Bozan the help given on the CLSM microscope and the software analysis. The authors are grateful for using the FE-SEM and the sputter-coater facility within the ProVIS - Centre for Chemical Microscopy by the Helmholtz - Centre for Environmental Research, Leipzig, which is supported by the European Regional Development Fund (ERDF, operational programme for Saxony), and the Helmholtz Association. This work was supported by the Helmholtz-Association in the frame of the Integration Platform “Tapping nature’s potential for sustainable production and a healthy environment” at the UFZ.

References:

[1] L. Shi, H. Dong, G. Reguera, H. Beyenal, A. Lu, J. Liu, H.-Q. Yu, J.K. Fredrickson, Extracellular electron transfer mechanisms between microorganisms and minerals, Nat Rev Microbiol. 14 (2016) 651–662. https://doi.org/10.1038/nrmicro.2016.93.

[2] M.E. Hernandez, D.K. Newman, Extracellular electron transfer, Cell Mol Life Sci. 58 (2001) 1562–1571. https://doi.org/10.1007/PL00000796.

[3] Z.M. Summers, H.E. Fogarty, C. Leang, A.E. Franks, N.S. Malvankar, D.R. Lovley, Direct Exchange of Electrons Within Aggregates of an Evolved Syntrophic Coculture of Anaerobic Bacteria, Science. 330 (2010) 1413–1415. https://doi.org/10.1126/science.1196526.

[4] D.R. Lovley, Electromicrobiology, Annual Review of Microbiology. 66 (2012) 391–409. https://doi.org/10.1146/annurev-micro-092611-150104.

[5] F. Caccavo, D.J. Lonergan, D.R. Lovley, M. Davis, J.F. Stolz, M.J. McInerney, Geobacter sulfurreducens sp. nov., a hydrogen- and acetate-oxidizing dissimilatory metal-reducing microorganism, Applied and Environmental Microbiology. 60 (1994) 3752–3759. https://doi.org/10.1128/aem.60.10.3752-3759.1994.

[6] M.D. Yates, S.M. Strycharz-Glaven, J.P. Golden, J. Roy, S. Tsoi, J.S. Erickson, M.Y. El-Naggar, S.C. Barton, L.M. Tender, Measuring conductivity of living Geobacter sulfurreducens biofilms, Nature Nanotech. 11 (2016) 910–913. https://doi.org/10.1038/nnano.2016.186.

[7] G.L. Chadwick, F.J. Otero, J.A. Gralnick, D.R. Bond, V.J. Orphan, NanoSIMS imaging reveals metabolic stratification within current-producing biofilms, PNAS. 116 (2019) 20716–20724. https://doi.org/10.1073/pnas.1912498116.

[8] C. Leang, M.V. Coppi, D.R. Lovley, OmcB, a c-Type Polyheme Cytochrome, Involved in Fe(III) Reduction in Geobacter sulfurreducens, Journal of Bacteriology. 185 (2003) 2096–2103. https://doi.org/10.1128/JB.185.7.2096-2103.2003.

[9] T. Mehta, M.V. Coppi, S.E. Childers, D.R. Lovley, Outer Membrane c-Type Cytochromes Required for Fe(III) and Mn(IV) Oxide Reduction in Geobacter sulfurreducens, Applied and Environmental Microbiology. 71 (2005) 8634–8641. https://doi.org/10.1128/AEM.71.12.8634-8641.2005.
[10] C.S. Stephen, E.V. LaBelle, S.L. Brantley, D.R. Bond, Abundance of the Multiheme c-Type Cytochrome OmcB Increases in Outer Biofilm Layers of Electrode-Grown Geobacter sulfurreducens, PLOS ONE. 9 (2014) e104336. https://doi.org/10.1371/journal.pone.0104336.
[11] J.M. Dantas, L. Morgado, M. Aklujkar, M. Bruix, Y.Y. Londer, M. Schiffer, P.R. Pokkuluri, C. Salgueiro, Rational engineering of Geobacter sulfurreducens electron transfer components: a foundation for building improved Geobacter-based bioelectrochemical technologies, Front. Microbiol. 0 (2015). https://doi.org/10.3389/fmicb.2015.00752.
[12] T.H. Yang, M.V. Coppi, D.R. Lovley, J. Sun, Metabolic response of Geobacter sulfurreducens towards electron donor/acceptor variation, Microbial Cell Factories. 9 (2010) 90. https://doi.org/10.1186/1475-2859-9-90.
[13] D.G. Brown, J. Komlos, P.R. Jaffé, Simultaneous Utilization of Acetate and Hydrogen by *Geobacter sulfurreducens* and Implications for Use of Hydrogen as an Indicator of Redox Conditions, Environ. Sci. Technol. 39 (2005) 3069–3076. https://doi.org/10.1021/es048613p.
[14] G. Bratbak, I. Dundas, Bacterial dry matter content and biomass estimations, Appl Environ Microbiol. 48 (1984) 755–757. https://doi.org/10.1128/aem.48.4.755-757.1984.
[15] M. Loferer-Krößbacher, J. Klima, R. Psenner, Determination of Bacterial Cell Dry Mass by Transmission Electron Microscopy and Densitometric Image Analysis, Appl Environ Microbiol. 64 (1998) 688–694. https://www.ncbi.nlm.nih.gov/pmc/articles/PMC106103/ (accessed August 18, 2021).
[16] C.E.A. Engel, D. Vorländer, R. Biedendieck, R. Krull, K. Dohnt, Quantification of microaerobic growth of Geobacter sulfurreducens, PLOS ONE. 15 (2020) e0215341. https://doi.org/10.1371/journal.pone.0215341.
[17] F. Harnisch, K. Rabaey, The Diversity of Techniques to Study Electrochemically Active Biofilms Highlights the Need for Standardization, ChemSusChem. 5 (2012) 1027–1038. https://doi.org/10.1002/cssc.201100817.
[18] N. Lebedev, S.M. Strycharz-Glaven, L.M. Tender, Spatially Resolved Confocal Resonant Raman Microscopic Analysis of Anode-Grown Geobacter sulfurreducens Biofilms, ChemPhysChem. 15 (2014) 320–327. https://doi.org/10.1002/cphc.201300984.
[19] Y. Liu, H. Kim, R.R. Franklin, D.R. Bond, Linking Spectral and Electrochemical Analysis to Monitor c-type Cytochrome Redox Status in Living Geobacter sulfurreducens Biofilms, ChemPhysChem. 12 (2011) 2235–2241. https://doi.org/10.1002/cphc.201100246.
[20] F. Scarabotti, L. Rago, K. Bühler, F. Harnisch, The electrode potential determines the yield coefficients of early-stage Geobacter sulfurreducens biofilm anodes, Bioelectrochemistry. 140 (2021) 107752. https://doi.org/10.1016/j.bioelechem.2021.107752.
[21] A.M. Nowicka, U. Hasse, G. Sievers, M. Donten, Z. Stojek, S. Fletcher, F. Scholz, Selective Knockout of Gold Active Sites, Angewandte Chemie. 122 (2010) 3070–3073. https://doi.org/10.1002/ange.201000485.
[22] A.M. Nowicka, U. Hasse, M. Hermes, F. Scholz, Hydroxyl Radicals Attack Metallic Gold, Angewandte Chemie International Edition. 49 (2010) 1061–1063. https://doi.org/10.1002/anie.200906358.
[23] W.E. Balch, G.E. Fox, L.J. Magrum, C.R. Woese, R.S. Wolfe, Methanogens: reevaluation of a unique biological group., Microbiological Reviews. 43 (1979) 260–296. https://doi.org/10.1128/MMBR.43.2.260-296.1979.
[24] D.R. Lovley, R.C. Greening, J.G. Ferry, Rapidly growing rumen methanogenic organism that synthesizes coenzyme M and has a high affinity for formate, Applied and Environmental Microbiology. 48 (1984) 81–87. https://doi.org/10.1128/aem.48.1.81-87.1984.

[25] S.A. Patil, F. Harnisch, B. Kapadnis, U. Schröder, Electroactive mixed culture biofilms in microbial bioelectrochemical systems: The role of temperature for biofilm formation and performance, Biosensors and Bioelectronics. 26 (2010) 803–808. https://doi.org/10.1016/j.bios.2010.06.019.
[26] S. Patil, F. Harnisch, U. Schröder, Toxicity Response of Electroactive Microbial Biofilms-A Decisive Feature for Potential Biosensor and Power Source Applications, Chem. Eur. J. of Chem. Phys. 11 (2010) 2834–2837. https://doi.org/10.1002/cphc.201000218.
[27] P. Champigneux, C. Renault-Sentenac, D. Bourrier, C. Rossi, M.-L. Delia, A. Bergel, Effect of surface roughness, porosity and roughened micro-pillar structures on the early formation of microbial anodes, Bioelectrochemistry. 128 (2019) 17–29. https://doi.org/10.1016/j.bioelechem.2019.03.002.
[28] Y. Liu, H. Kim, R. Franklin, D.R. Bond, Gold line array electrodes increase substrate affinity and current density ofelectricity-producing G. sulfurreducens biofilms, Energy and Environmental Science. 3 (2010) 1782–1788. https://doi.org/10.1039/c0ee00242a.
[29] B. Korth, A. Kuchenbuch, F. Harnisch, Availability of Hydrogen Shapes the Microbial Abundance in Biofilm Anodes based on Geobacter Enrichment, ChemElectroChem. 7 (2020) 3720–3724. https://doi.org/10.1002/celc.202000731.
[30] E. Marsili, J. Sun, D.R. Bond, Voltammetry and Growth Physiology of Geobacter sulfurreducens Biofilms as a Function of Growth Stage and Imposed Electrode Potential, Electroanalysis. 22 (2010) 865–874. https://doi.org/10.1002/elan.200800007.
[31] L. Peng, Y. Zhang, Cytochrome OmcZ is essential for the current generation by Geobacter sulfurreducens under low electrode potential, Electrochimica Acta. 228 (2017) 447–452. https://doi.org/10.1016/j.electacta.2017.01.091.
[32] M. Füeg, Z. Borjas, M. Estevez-Canales, A. Esteve-Núñez, I.V. Pobelov, P. Broekmann, A. Kuzume, Interfacial electron transfer between Geobacter sulfurreducens and gold electrodes via carboxylate-alkanethiol linkers: Effects of the linker length, Bioelectrochemistry. 126 (2019) 130–136. https://doi.org/10.1016/j.bioelechem.2018.11.013.
[33] E.D. Kees, C.E. Levar, S.P. Miller, D.R. Bond, J.A. Gralnick, A.M. Dean, Survival of the first rather than the fittest in a Shewanella electrode biofilm, Commun Biol. 4 (2021) 1–9. https://doi.org/10.1038/s42003-021-02040-1.
[34] F. Harnisch, B. Korth, First settlers persist, Joule. 5 (2021) 1316–1319. https://doi.org/10.1016/j.joule.2021.05.022.